ELSEVIER

Empirical Methods To Compensate for a View-Angle-Dependent Brightness Gradient in AVIRIS Imagery

Robert E. Kennedy, Warren B. Cohen,† and Gen Takao‡*

A view-angle-dependent brightness gradient was observed in an AVIRIS image of a forested region in Oregon's Cascade Mountains. A method of removing the view-angle effect was sought that would not alter the radiometric integrity of the image, and which would require minimal ancillary information. Four methods were tested and evaluated in terms of remaining brightness gradient and in terms of retention of spectral characteristics. All methods used a quadratic fitting equation to model the changes in brightness across view angles. Other descriptive coefficients were calculated to aid in interpretation. The observed view-angle effect varied with wavelength in a manner consistent with predictions of bidirectional reflectance distribution function characteristics for vegetation. View-angle effects were determined to contain both additive and multiplicative components, with multiplicative components being strong in the chlorophyll absorption region. The view-angle effect in a given pixel was a function of both an underlying view-angle response determined by surface structure and the inherent brightness of that pixel. The most successful compensation method was the one that best accounted for broad differences between pixels in these two components. Despite the simplifying assumptions necessary for empirical view-angle correction techniques, they can still be useful for hyperspectral remote-sensing data in situations where the view-angle brightness variations would mask variance useful for extracting scene information. Published by Elsevier Science Inc., 1997

* Department of Forest Science, Oregon State University, Forestry Sciences Laboratory, Corvallis

† USDA/Forest Service, Pacific Northwest Research Station, Forestry Sciences Laboratory, Corvallis

‡ Remote Sensing Laboratory, Forestry and Forest Products Research Institute, Ministry of Agriculture, Forestry and Fisheries, Tsukuba, Japan

Address correspondence to Warren Cohen, USDA/Forest Service, Pacific Northwest Research Station, Forestry Sciences Lab., 3200 SW Jefferson Way, Corvallis, OR 97331.

Received 17 December 1996; revised 20 June 1997.

REMOTE SENS. ENVIRON. 62:277–291 (1997)
Published by Elsevier Science Inc., 1997
655 Avenue of the Americas, New York, NY 10010

INTRODUCTION

The Airborne Visible Infrared Imaging Spectrometer (AVIRIS) was designed to capture subtle spectral features of ground targets using narrow spectral bandwidths and full-spectrum (0.48–2.50 μm) coverage (Vane et al., 1993). One proposed use has been the discrimination of tree species by detection of canopy chemistry signatures (Martin, 1994; Martin et al., 1996). A study was begun to investigate the feasibility of using AVIRIS data to discriminate species in coniferous forests of the Cascade Mountains of western Oregon. During preprocessing, however, a strong brightness gradient was observed that spanned the cross-track dimension of the image, and which was associated with variation in sensor view-angle rather than with a surficial trend or patterning of landscape types (Fig. 1). Concerned that the low-amplitude spectral features necessary for species discrimination would be masked, we sought a generally applicable method of correction that would minimize the brightness gradient in AVIRIS data while retaining the underlying spectral information. As a preprocessing step, such a correction method would ideally require little or no collection of ancillary information.

BACKGROUND

Compensating for Brightness Effects

Theory

Radiometric distortions may be eliminated by modeling of first principles, by applying a band ratio, or by apply-

0034-4257/97/$0.00
PII S0034-4257(97)00111-9

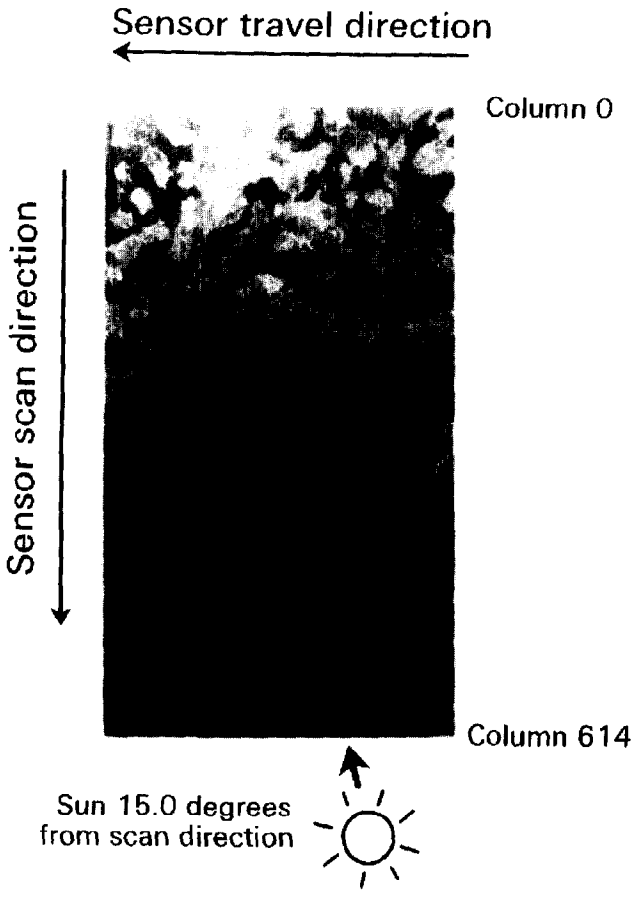

Figure 1. Portion of a 19 July 1994 AVIRIS image (wavelength 0.55 μm) near the H. J. Andrews Experimental Forest, Oregon, showing view-angle dependent brightness gradient. Plane of sun is 15.0° from the plane of the scanning sensor (nearly perpendicular to flight path of aircraft). Clearcuts are lighter than surrounding forest. Note that clearcuts at the bottom of the image (toward the sun; higher column numbers) are nearly as dark as forested areas in the top of the image (lower column numbers).

ing a scene-dependent empirical correction (Irons and Labovitz, 1982; Leckie, 1987). The former is often impractical for investigations where characterization of the effect is not the final goal. The second option has proven useful in reducing such effects (Nalepka and Morgenstern, 1972; Royer et al., 1985; Kleman, 1987; Qi et al., 1995), but was not desirable in this study because the original spectral characteristics were desired as output for other analyses. Thus an empirical route was chosen.

Empirical approaches are based on the following model of observed radiance:

observed radiance=target radiance+distortions.

Empirical methods seek to minimize the distortions, which are a function of many factors, such as sensor view-angle and altitude, wavelength, and the angle between sun azimuth and sensor scan plane (Irons and Labovitz, 1982; Royer et al., 1985; Irons et al., 1987; Kleman, 1987). Many of these remain constant for a single image and cannot be removed by evaluation of within-scene variation. The view-angle, however, changes for every pixel in a scan line. Each increment in view-angle increases the quantity of atmosphere through which the sensor must view, which in many cases increases path radiance and, consequently, overall brightness at wide view-angles (Royer et al., 1985; Irons et al., 1987; Leckie, 1987). Each change in view-angle also alters the sun–viewer–object geometry of the surface objects being viewed, the effects of which can be modeled with a bidirectional reflectance distribution function (BRDF; Hugli and Frei, 1981; Royer et al., 1985; Walthall et al., 1985). For a given wavelength and surface type, BRDF can cause either increased or decreased observed radiance at greater view-angles, depending on sun–sensor–object geometry. It is especially strong when the sensor is scanning in the plane of the sun (Ranson et al., 1994). Cross-track brightness gradients are considered to be a combination of these two view-angle-dependent effects, that is,

brightness gradient (a)=*path radiance* (a)+*BRDF* (a)

where a is the view-angle (Leckie, 1987; Irons et al., 1991). Empirical compensation for the brightness gradient does not require that these two components be separated, merely that the observed brightness gradient be modeled and removed.

The brightness gradient is often modeled by calculating mean radiance by view-angle $[\bar{L}(a)]$ and fitting a quadratic curve fit to the means (Staenz et al., 1981; Brown et al., 1982; Leckie, 1987):

$$\hat{L}(a)=qa^2+la+c, \quad (1)$$

where $\hat{L}(a)$ is fitted mean radiance for a given angle and q, l, and c are estimates of the quadratic, linear, and constant fitting coefficients, respectively. Knowing that view-angle effects are zero when the view-angle is zero (i.e., at the nadir), compensation factors can be calculated that will normalize each view-angle to the nadir view using an additive or multiplicative compensation factor:

$$k_1(a)=\hat{L}(a)-\hat{L}(a=0), \quad (2)$$

$$k_2(a)=\hat{L}(a)/\hat{L}(a=0), \quad (3)$$

(Leckie, 1987), where $\hat{L}(a=0)$ is the fitted mean radiance at the nadir and $k_1(a)$ and $k_2(a)$ are the additive and multiplicative compensation factors, respectively, for a. A pixel at position (a,y), where y is the row number in the along-track dimension of the image, has an observed radiance $L_{(a,y)}$. It is assigned a corrected radiance, $L'_{(a,y)}$, using one of the two compensation factors:

$$L'(a,y)=L'(a,y)-k_1(a), \quad (4)$$

$$L'(a,y)=L(a,y)/k_2(a). \quad (5)$$

Radiometric Implications

Both additive and multiplicative corrections have been used previously (Brown et al., 1982; Staenz et al., 1986;

Leckie, 1987), but there is disagreement about which technique is more appropriate. The multiplicative approach will compress the standard deviation of radiance at a given a in proportion to the size of $k_2(a)$. If standard deviation is assumed to be unrelated to mean radiance, then the standard deviation compression caused by the multiplicative approach will introduce unwanted error and should thus be avoided (Irons and Labovitz, 1982). If standard deviation is assumed to be directly proportional to mean radiance, however, then standard deviation of radiance should be compressed and the additive approach should be avoided (Royer et al., 1985). Neither assumption has been tested in the context of applying an empirical view-angle compensation.

BRDF Considerations

Before a mathematical correction procedure is applied, a choice must be made about the population of pixels from which to draw the mean radiance for each view-angle, $\bar{L}(a)$. Since the BRDF component of the view-angle effect is dependent on the type of surface being viewed (Kriebel, 1978; Cihlar et al., 1994; Deering et al., 1994), a separate fitting equation [Eq. (1)] is expected for each type of surface component. Applying the fitting equation from one surface type to another surface type can result in inaccurate compensation (Leckie, 1987), the severity of which would increase as the difference in BRDF between surface types increases. This can be alleviated by limiting research to one type of surface (Treitz et al., 1985; Leckie, 1987; Johnson, 1994), or by partitioning the image into classes and treating each class separately (Leckie et al., 1995). Unless extensive measurements are used to calculate BRDF characteristics for all scene components (Hugli and Frei, 1981), pre-classification must be based on theoretical assumptions.

Objectives for This Study

As no single empirical view-angle compensation method is without drawbacks, we decided to test several methods for our study area. We expected that the study area would accentuate differences between methods, since it contained an intimate mixture of surface types with theoretically extreme differences in BRDF (i.e., bare-ground and regrowing clearcuts in a matrix of mature and old-growth coniferous forest). In the course of testing methods, it was hoped that the high spectral resolution of AVIRIS would contribute to general understanding of the wavelength dependence of view-angle effects.

DATA ANALYSIS

Preprocessing

The AVIRIS instrument is a hyperspectral, airborne, whisk-broom type sensor (Vane et al., 1993). Radiance in 224 contiguous wavebands is recorded simultaneously for each pixel in an image. Waveband centers are approximately 10 nm apart, running from 0.48 μm to 2.5 μm. The maximum view-angle from nadir is 15.0°. Pixels represented an area on the ground approximately 18 m on a side.

Atmospheric effects were addressed with ATREM (ATmospheric REMoval program for AVIRIS data; Gao et al., 1993), using aerosol optical thickness estimates from sun photometer readings taken at the site on the day of image acquisition. Because no ground-based spectrometer measurements were available for validation, apparent surface reflectance derived from ATREM was acknowledged to be only an approximation of true reflectance. ATREM does not correct view-angle effects.

From the 224 wavebands of the AVIRIS data, 154 waveband images were selected that did not display water vapor absorption noise or detector noise problems. In each waveband, the image had 1288 scan lines with 614 scan angles per scan line. Each scan angle was assigned a column value; each scan line was assigned a row value. The brightness effect stretched across dimension of the 614 columns (Fig. 1).

Study Area and Illumination Geometry

AVIRIS imagery included the H. J. Andrews Experimental Forest and adjacent areas (Table 1). The area is characterized by rugged topography having an intimate mixture of high and low biomass densities: old-growth coniferous forests, with extremely high biomass (up to 650×10^6 g C/ha above- and below-ground pools; Grier and Logan, 1977) and complex vertical and horizontal canopy structure, juxtaposed to clearcuts, with little or no live biomass and significant exposed soil.

Table 1 presents data relevant to sun and view-angle geometry and aircraft directional characteristics for the day of the image acquisition. The scanning plane was nearly parallel to the plane of the sun (Fig. 1), providing for maximum predicted BRDF effects.

View-Angle Compensation

Strategies To Be Tested

A compensation strategy can use either additive or multiplicative compensation, and can derive mean radiance either from the whole image or from classified subsets. From unique combinations of these options arose four view-angle compensation methods, named hereafter as the additive-unclassified, additive-classified, multiplicative-unclassified, and multiplicative-classified methods.

Classification

For the two classified methods, the image was partitioned into broad "BRDF classes" chosen based on theoretical expectations. In the system of study, two axes of variation were expected to cause variations in BRDF: 1) percent of pixel dominated by soil or vegetation (Nor-

Table 1. Data from AVIRIS Flight over H. J. Andrews Experimental Forest

Study site location	44°17′N, 122°18′W
Elevation	400–1500 m, mean ~800 m
Time and date of image	12:48 p.m. local time, 19 July 1993
Ground element (pixel size)	~18 m
Aircraft heading[a]	273.5°
Scan angle[a]	3.5° for northern half of image, 183.5° for southern half
Sun angle[a]	168.5° azimuth, 23.4° zenith

[a] Geographic north=0°.

man et al., 1985; Ranson et al., 1985), and 2) degree of canopy heterogeneity within the vegetative canopies (Li and Strahler, 1986; Kleman, 1987, although see Kimes et al., 1986 for context). Twenty classes were derived from an iterative optimization classification; these were then reduced to three classes along these two axes of variation. Class 1 represented the soil-dominated areas in the image and was found exclusively in recent clearcuts and burns. Classes 2 and 3 both occupied the vegetation-dominated portion of the soil–vegetation axis, but differed in their canopy heterogeneity. Class 2 consisted of hardwood and young conifer that would appear relatively "smooth" within a given pixel element. Class 3 contained mature and old-growth conifer forests with significant canopy structural complexity at the scale of the sensor pixel.

For this image, 11.2% of the pixels were in Class 1, 27.4% in Class 2, and 61.4% in Class 3. The categories were well distributed across the brightness gradient of the image.

In both the additive- and the multiplicative-classified methods, each of the three classes was treated separately for all of the following view-angle compensation methods. At the end of the compensation process, the three groups were recombined into a single image. For both of the unclassified image methods, all of the following methods apply.

Fitting the Mean Reflectance Curve and Calculating Interpretive Coefficients

For ease of interpretation, pixel reflectance values as calculated by ATREM were used in place of radiance for Eqs. (1)–(5) above. A preliminary test showed that ATREM had no effect on view-angle characteristics.

Mean reflectances for the 614 columns were fit according to Eq. (1) for all 154 wavebands using column number as a surrogate for view-angle (a). Coefficients of determination for the fit of the quadratic equation to the observed means were also calculated.

In keeping with the goal of simplicity, the effects of autocorrelation between columns (Irons and Labovitz, 1982) and the potential for using higher-order or physically based fitting equations were ignored (Irons and Labovitz, 1982; Teillet et al., 1985; Walthall et al., 1985). Addressing autocorrelation or developing physically based models would be beyond the desired scope of the methodology; determining higher-order fitting equations for each of 154 bands would be impractical.

The coefficients of Eq. (1) were manipulated to create two new interpretive coefficients. The first, named the nadir-adjusted view-angle curvature, or q', was designed to allow comparison of curvature of the view-angle effect (q) between bands. If q is proportional to the mean brightness of a band, then comparisons of q between wavebands could be affected more by average band brightness than by actual curvature of the view-angle effect. To reduce this potential error and aid in interpretation, q was divided by the fitted mean reflectance at the nadir (where view-angle effects are zero) for each band, resulting in the coefficient q'. A second interpretive coefficient was designed to track the interactions of two predicted BRDF effects (Kimes, 1983; see the Discussion section for a description). Their relative strengths alter the column at which quadratic equation [Eq. (1)] reaches its minimum predicted reflectance:

$$x_{(min)} = \frac{-l}{2q}. \tag{6}$$

A final pair of interpretive coefficients assessed the mathematical validity of using the multiplicative or additive approaches. For each of the 154 bands, mean reflectance for all pixels in each of the 614 columns was plotted against the standard deviation in reflectance values for pixels in each of those columns, and a simple least-squares regression line was fit to the 614 data points. The slope of the regression line is designated as $m_{(stddv)}$ and the intercept as $i_{(stddv)}$. A positive slope with a zero intercept would indicate a strictly proportional (multiplicative) relationship between standard deviation of brightness and brightness, implying that the multiplicative correction methods were mathematically valid. A zero slope, with a nonzero intercept, would indicate no relationship between the standard deviation of brightness and brightness, and would support the use of an additive approach. Because brightness offsets introduced or unaccounted for by ATREM were unknown, neither $m_{(stddv)}$ nor $i_{(stddv)}$ could be used as a precision measurement, but rather as an indicator of trends.

Calculation of Compensation Factors and Correction of Images

An additive compensation factor $k_1(x)$ and a multiplicative compensation factor $k_2(x)$ were calculated according to Eqs. (2) and (3), respectively, for x=1–614 columns. Images were corrected according to Eqs. (4) and (5) for the additive- and multiplicative-type corrections, respectively. For the two classified methods, only the compensation factor appropriate to a given pixel's BRDF class was applied to that pixel.

Evaluation

The methods were evaluated and compared against each other according to the following criteria:

1. Did the image still display a noticeable brightness gradient?
2. Was the spectral integrity of image data maintained?

The first test was a visual comparison of the spatial distribution of brightness before and after compensation. The compensation methods operate on a column-by-column basis; if average brightness compensation was achieved by overcompensating some rows within a column while undercompensating other rows, then the compensation method was not useful. An image-wide comparison of all columns and rows would reveal patterns in over- or undercompensation.

The second test evaluated whether spectral shape was preserved by the compensation procedures. Compensation was performed one band at a time, without reference to conditions in the preceding or subsequent waveband. Only if the brightness relationships *between* bands were maintained would the spectral information be preserved. To examine spectral preservation, mean spectra for nine-pixel test regions at three view-angles along the brightness gradient were compared before and after compensation for all three BRDF classes. Spectra after compensation were compared against the original spectra for maintenance of low-frequency spectral features (general spectral shape). High-frequency spectral features were examined by comparing pseudo-first-derivatives of spectral response, calculated according to Martin (1994).

RESULTS

Extracting and Fitting Brightness Curves

Unclassified Image

As can be expected from a forested region, mean reflectances across wavelengths were dominated by the spectral signal of vegetation, with distinctive chlorophyll absorption evident at 0.68 μm, high reflectance in the near infrared, and intermediate reflectance in the 1.5–1.8 μm water absorption region (Fig. 2a). The fit of the quadratic equation to the observed mean reflectances across columns (Fig. 2b) was good, with r^2 values greater than 0.9 for all wavebands (data not shown). Interpretive coefficients follow the patterns described in the next section for Classes 2 and 3 of the classified image.

Classified Image

For Classes 2 and 3 of the classified image, the spectral character of the coefficients q, q', and $x_{(min)}$ appeared to be significantly related to vegetation (Figs. 3a, b, and c). The coefficient q takes the unmistakable shape of a generic vegetation spectrum (Fig. 3a). The shapes of q' and $x_{(min)}$ (Figs. 3b and c), while not strictly vegetative, are characterized by spectral features that correspond to wavelengths of critical vegetation features, especially the chlorophyll wavelengths (0.68 μm) and the red–near-infrared transition (0.68 μm to ~0.90 μm). The fact that the view-angle-dependent curvature existed within the vegetative classes reconfirms the observation that the brightness effect was related to view-angle, rather than to patterning of bright and dark classes on the landscape. The soil-dominated class (Class 1) behaved differently for all coefficients (Figs. 3a–c; note that $x_{(min)}$ was mathematically uninterpretable where q approached zero). Notable is the shape of q', which for Class 1 was a rough mirror-image from q' from the two vegetative classes. The values of r^2 for the fit of quadratic equation were uniformly high for the vegetative classes, but poorer for Class 1, especially at the chlorophyll absorption region and the two mid-infrared regions (Fig. 4).

The relative strength of the additive and multiplicative assumptions, as indicated by $i_{(stddv)}$ and $m_{(stddv)}$, respectively, also appeared to respond to absorption characteristics of vegetation, although they were quite variable between classes and across wavelengths (Fig. 5). A notable point of agreement between the classes was a peak in the appropriateness of *both* the multiplicative and additive assumptions at the chlorophyll absorption region.

Summary

Three major patterns emerged from the investigation of the interpretive coefficients:

1. The character of the brightness gradient across wavelengths appeared to be connected to the spectral characteristics of vegetation.
2. The brightness gradient in the soil-dominated class (Class 1) was quite different from the two vegetated classes.
3. The strength of the multiplicative and additive assumptions varied with wavelength; both effects were present to varying degrees at most wavelengths.

Evaluating the View-Angle Compensation Methods

Does the Resultant Image Retain a Visible Brightness Gradient?

In comparing images after application of the four compensation methods, seven representative wavebands were evaluated for image contrast and for distribution of brightness gradient among cover types. The classified methods performed better across bands than did the unclassified methods. For both the classified and unclassified methods, the multiplicative versions performed better than their additive counterparts. A cross-track subset of a green waveband image (0.55 μm) is used as a visual example, showing the original image (Fig. 6a) and images from all four of the compensation methods (Figs. 6b–e) displayed according to the same brightness stretching

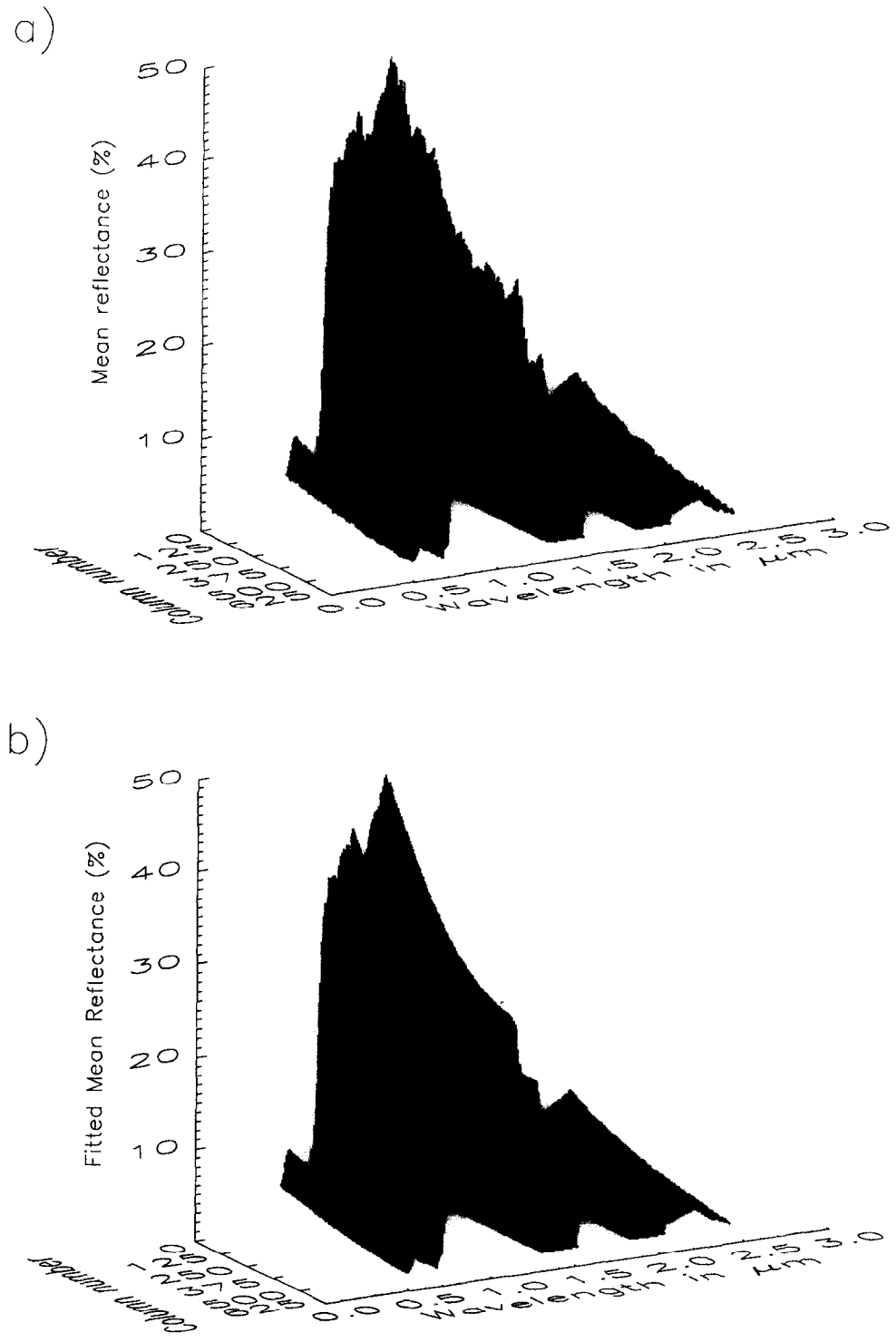

Figure 2. Reflectances by wavelength and image column number for the 19 July 1994 AVIRIS image (a portion of which is shown in Fig. 1). Each column number corresponds to a different scan angle of the sensor; column numbers greater than 306 (the nadir point) are those where the sensor was aimed towards the sun. a) Mean image values taken from 1288 pixels at each column number. b) The values in a) fitted according to a quadratic equation [Eq. (1)], using column number as independent variable and mean reflectance as dependent variable. Each wavelength is fit separately. Reflectance values are calculated from raw data using ATREM (Gao et al., 1993).

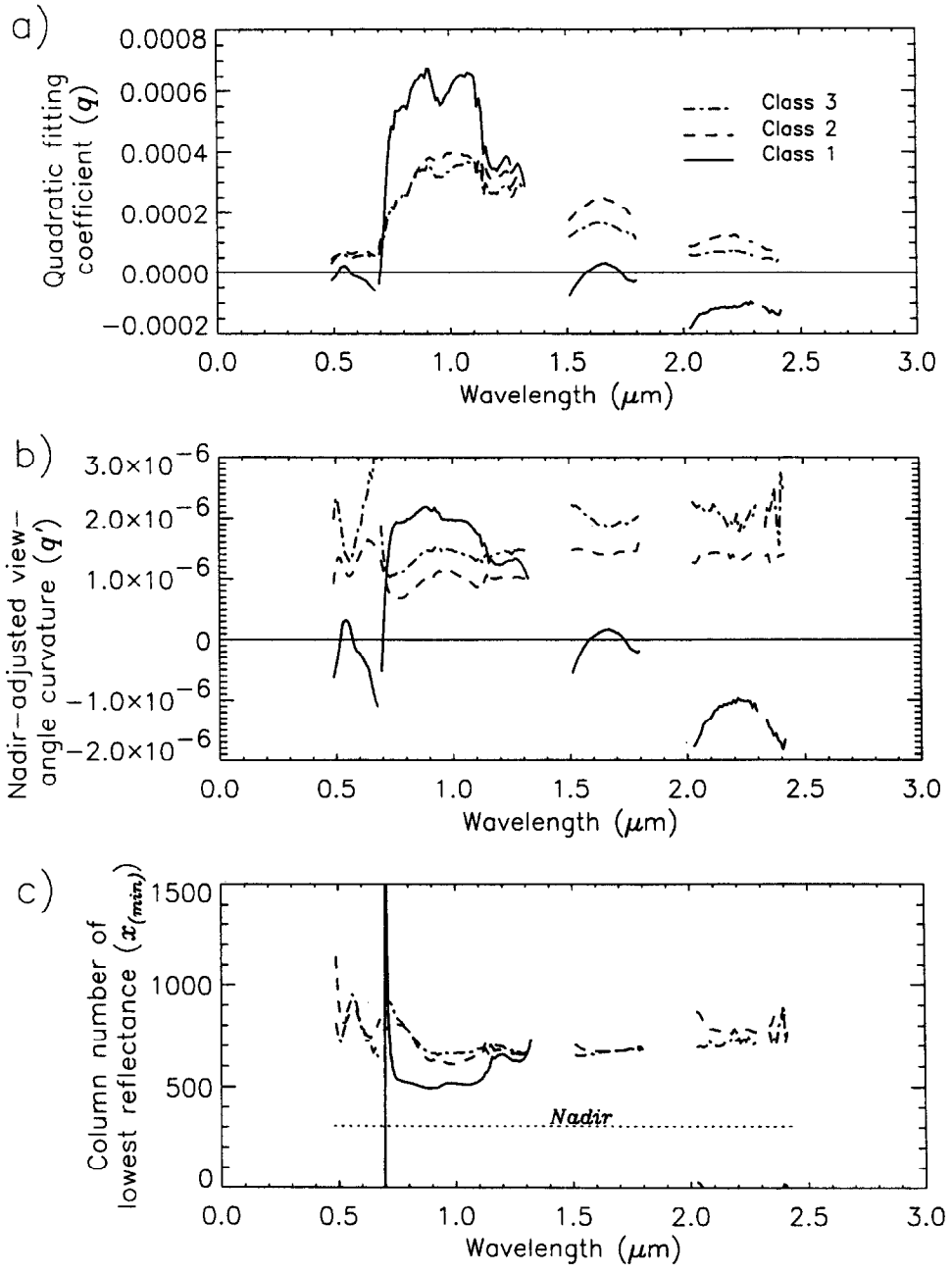

Figure 3. Interpretive coefficients derived from the fit of the quadratic equation for Classes 1, 2, and 3. a) The quadratic term q in the quadratic equation [Eq. (1)]. Higher q indicates a stronger view-angle effect. b) Nadir-adjusted view-angle curvature q' calculated by dividing q for a given band by fitted nadir reflectance in that band. This eliminates the effect of average band reflectance, allowing direct comparison of view-angle effects between bands. c) The column number where the fitted quadratic equation reaches a minimum, $x_{(min)}$. Nadir is column 306; higher values are on the sun-side of nadir. Because the curvature (q) for Class 1 drops below zero [see part a)], the mathematical assumptions for the calculation of $x_{(min)}$ are invalid for that class and cause $x_{(min)}$ to vary outside the meaningful bounds of this plot.

rules, along with the classified image for reference (Fig. 6f). The least effective method across bands was the additive-unclassified method, which consistently overcompensated for the brightness effect in Class 3. The multiplicative-unclassified method generally alleviated this problem, except in the two mid-infrared regions (not shown), where some undercompensation was evident. The two classified methods yielded well-balanced images, with high contrast and no patterns of inappropriate compensation.

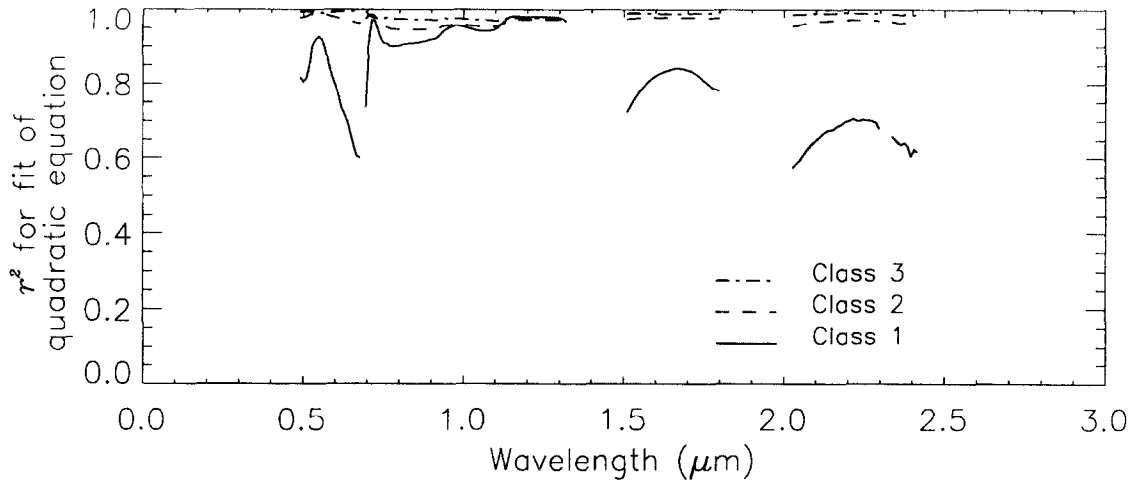

Figure 4. Coefficients of determination for the fit of the quadratic equation to mean reflectances derived from the three classes.

Was Spectral Integrity Maintained in Representative Test Regions?

Spectra from Class 1, 2, and 3 test regions were compared before and after application of all four compensation methods. Spectral pseudo-first-derivatives were nearly identical for all compensation methods (an example is shown in Fig. 7), indicating that fine-scale spectral features were well-maintained by all methods. Broad spectral features were also preserved for the test regions dominated by vegetation, including all of the test regions from Classes 2 and 3 (representative data for Class 2 shown in Fig. 8) and two of the test regions from Class 1 (not shown). The third test region from Class 1 was nearly pure soil and responded to the compensation methods in a manner unlike the other test regions (Fig. 9). For this test region, no compensation method fully maintained spectral integrity, especially in the transition from the red to the near-infrared wavelengths, although the multiplicative-classified method best maintained overall spectral shape.

DISCUSSION

Context of the Study

Because of its potential for improving canopy inversion models, the BRDF remains a subject of continued fruitful research, especially as the availability of variable look-angle sensors increases (Irons et al., 1991; Abuelgasim and Strahler, 1994). For single-pass, nadir-viewing instruments, however, the effects of BRDF and other view-angle effects can hinder processing. Building on work by other investigators using other instruments, this study evaluated four related empirical methods of compensating for view-angle effects in AVIRIS imagery. The conclusions of this study will be useful for situations where the brightness gradient is severe enough to mask variation in the original data, and where some means of compensation is required that both will be efficient and will cause minimal radiometric distortion.

Limitations and Potential Error Sources

The methodologies tested here have several limitations and limiting assumptions.

- They compensate for view-angle effects only, not for sun-angle effects that would vary between images acquired at different times.
- Although they brighten dark areas, they will not change the lower signal-to-noise ratio in dark areas.
- They make no explicit accounting for topography; however, there are no topographic features in this landscape that function at the scale of the swath-width of the sensor, so topographic effects likely explained some variation around the general view-angle trend but not the trend itself.
- They assume that a quadratic curve is the appropriate model for the brightness gradient; high r^2 values indicate that this was a reasonable assumption except for Class 1, which will be discussed in the subsection on BRDF predictions below.
- The multiplicative methods require the zero point on the reflectance scale to be absolutely accurate; without ground measurements, this was not testable.

Interpretation of View-Angle Effects

General Observations

From the investigation of the interpretive coefficients [q, q', $x_{(min)}$, $m_{(stddv)}$, $i_{(stddv)}$], several general trends are evident. First, all noticeable trends in the data appear to be related to vegetation's spectral features, not to atmospheric path

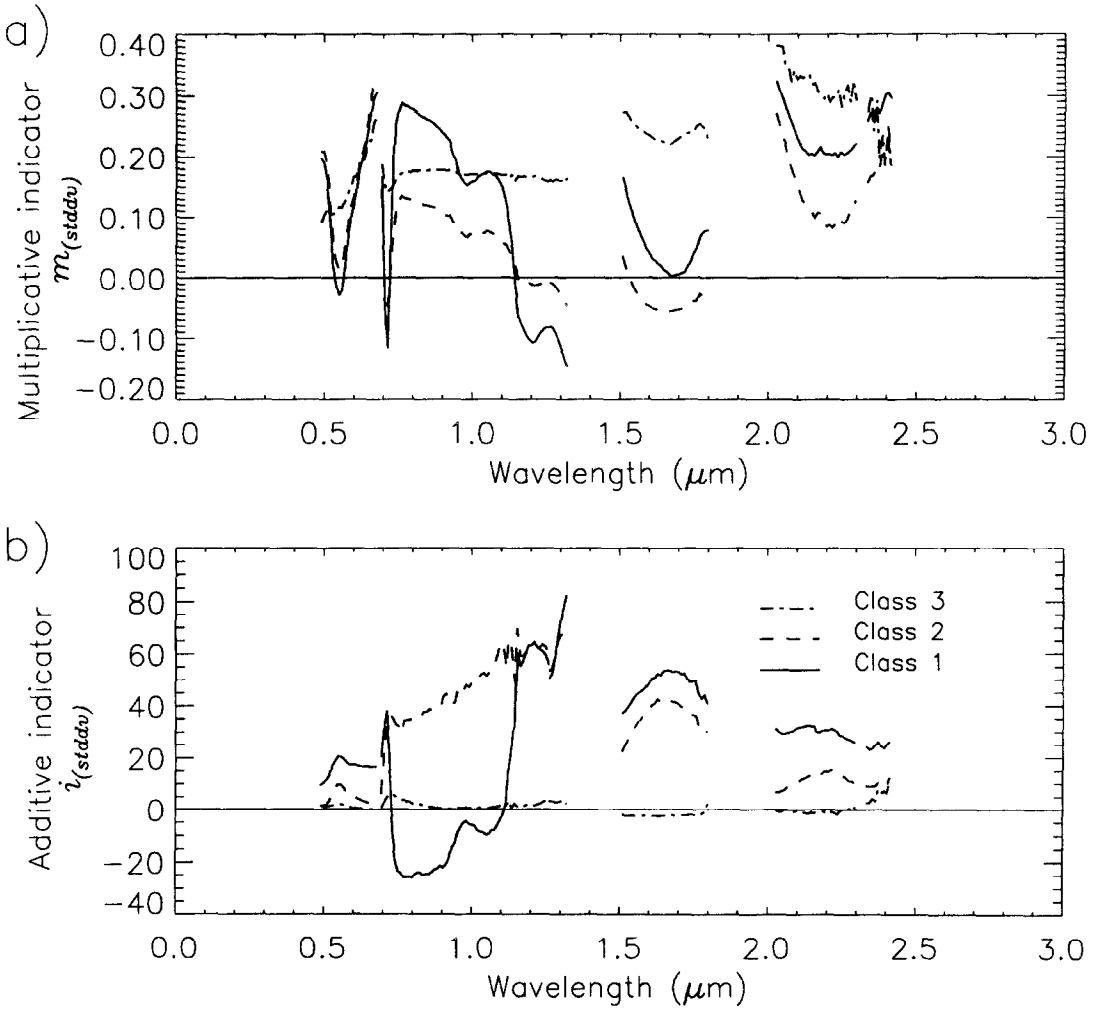

Figure 5. Coefficients for determining whether the standard deviation of reflectance is dependent on mean reflectance. For the 614 columns in each waveband, the former was plotted against the latter, and a linear regression line was fit to the relationship. The slope $m_{(stddv)}$ and y-intercept $i_{(stddv)}$ for the linear regression line are shown by wavelength. A nonzero slope indicates that standard deviation is partially proportional to mean brightness. A nonzero y-intercept indicates that some portion of the standard deviation is independent of mean brightness.

radiance effects, which are greatest in the blue wavelengths and gradually decrease as wavelength increases (Leckie, 1987). Although path radiance is additive and may be responsible for the observed additive relationship in view-angle effects [$i_{(stddv)}$], it clearly does not explain the bulk of the behavior of the view-angle effect. Second, the curvature of the view-angle effect is strongest in spectral regions where vegetation strongly absorbs radiation, and is weakest where vegetation scatters and transmits radiation. Finally, Class 1, with minimal vegetation, behaves uniquely in its response to view-angle changes. All three of these observations point to surface BRDF as the primary determinant of the view-angle effect.

BRDF

Kimes (1983) suggests that the BRDF for vegetated canopies is defined by the interaction of two effects. As view-angle increases from nadir, the probability of the sensor gaining a direct line of sight to dark, lower canopy components decreases, and the proportion of bright, upper canopy components in view increases. This causes a minimum reflectance at nadir with symmetric curvilinear increases in reflectance as view-angle increases in both directions (i.e., a quadratic curve). We refer to it as Effect 1. Effect 2 results from the sensor viewing forelit surfaces when looking away from the sun and viewing backlit surfaces when looking towards the sun. Unlike Effect 1, it causes a nearly linearly decreasing reflectance as view-angle moves from forelit to backlit surfaces. The combination of the two effects will produce a quadratic curve with a minimum point offset in the direction of backlighting, i.e. towards the sun.

In this study, the coefficients q' and $x_{(min)}$ are designed as indicators of Effect 1 and 2. The curvature

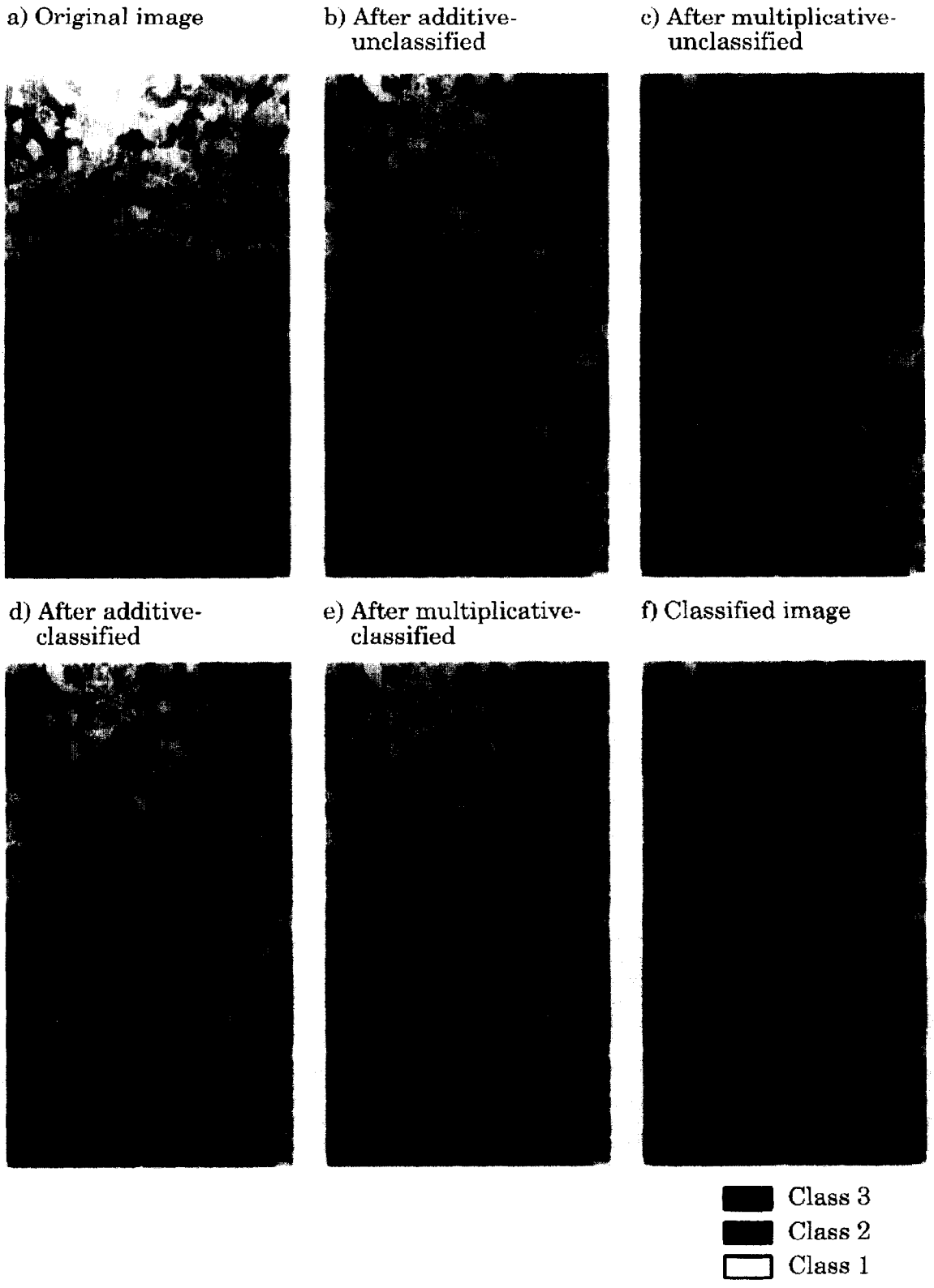

Figure 6. Example images comparing the image before and after compensation. a) Original image swath (at wavelength 0.55 μm). b–e) Image swaths resultant from the four view-angle compensation methods. f) The classified image used for both the additive- and multiplicative-classified compensation procedures. Column number (as used in previous figures) increases from bottom to top of the image; the nadir line runs horizontally across the middle of the image. The top portion of the image is on the backscatter side of nadir.

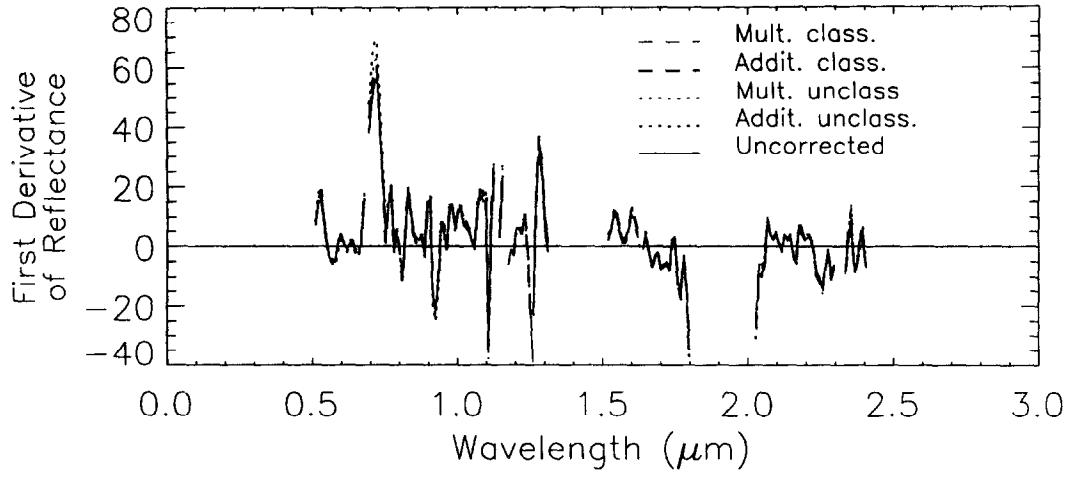

Figure 7. Spectral first derivatives for an example test site before and after application of compensation methods. The test site was from Class 2 on the forward scatter side of nadir (see Fig. 8c for associated spectra). There is essentially no difference between post-compensation and original-image first derivatives, indicating that fine-scale spectral information was retained by all compensation methods.

measured by q' should respond directly to Effect 1. The coefficient $x_{(min)}$ measures the interactions between Effects 1 and 2. As Effect 2 becomes stronger *relative* to the quadratic influence of Effect 1, the slope of its linear view-angle effect increases and the minimum point of the quadratic curve [$x_{(min)}$] moves further from nadir. This may occur either when Effect 2 strengthens or when Effect 1 weakens. Consequently, Effect 2 must be interpreted by examining trends in both q' and $x_{(min)}$.

Examining BRDF Predictions

Using q' and $x_{(min)}$ we can infer whether the predictions of Effect 1 and 2 adequately describe the brightness gradient. At wavelengths where canopy absorption is high, lower canopy components will be much darker than upper canopy components, and the higher contrast should accentuate Effect 1. Effect 2 should be driven by the relationship between leaf transmittance and reflectance: When leaf transmittance is low compared to reflectance, the backlit sides of leaves will be relatively dark, and Effect 2 will be strong; when transmittance and reflectance are on a par, Effect 2 will be weaker.

For vegetated classes (Classes 2 and 3) and for the unclassified image (with proportionally little soil), these predictions are accurate. Effect 1, as measured by q', is greater at wavelengths where vegetative absorption is higher [the chlorophyll region (0.68 μm) and the minor water absorption regions (1.5–1.8 μm)] and weaker where vegetative absorption is minimal [the near-infrared region (0.80–1.1 μm); Fig. 3b]. Differences between reflectance and transmittance for conifers are relatively small at most wavelengths (Daughtry et al., 1989; Williams, 1991), so the strength of Effect 2 should vary little across wavelengths. This appears to be the case here: Because $x_{(min)}$ changes in nearly direct opposition to q' (Fig. 3c), it appears that it is being altered strictly by changes in Effect 1 and that Effect 2 is relatively stable across wavelengths.

In the sparse canopies of Class 1, Effect 1 would be expected to play a lesser role than Effect 2. The changes in brightness with view-angle are therefore poorly described by a quadratic fit (low r^2 values, Fig. 4). Additionally, descriptive coefficients which assume a quadratic curvature, (q, q', and x_{min}), only describe that portion of the brightness gradient attributable to vegetation, making it impossible to say how well Effect 2 describes soil BRDF. Nevertheless, it is quite clear that BRDF in Class 1 is quite different from that in the vegetated classes.

BRDF in Sparse versus Dense Canopies

The stark contrast in BRDF characteristics between Class 1 and the vegetated classes indicates that for this scene, at least, the soil–vegetation axis caused more dramatic variations in BRDF than did the vegetative structural complexity. This is consistent with the conclusion of Kimes et al. (1986) that homogenous closed canopies, whether forest or grassland, should manifest BRDF effects that are similar to each other and different from soil-dominated regions of any type.

Evaluation of Compensation Methods

Validity of the Additive and Multiplicative Compensation Techniques

The coefficients $m_{(stddv)}$ and $i_{(stddv)}$ were intended to measure the validity of using the multiplicative or additive approaches. Their statistical robustness was questionable in Class 3 due to the presence of two distinct clusters of pixels in standard deviation/brightness space (not shown). Nevertheless, Class 1 and 2 did not show subclasses, but

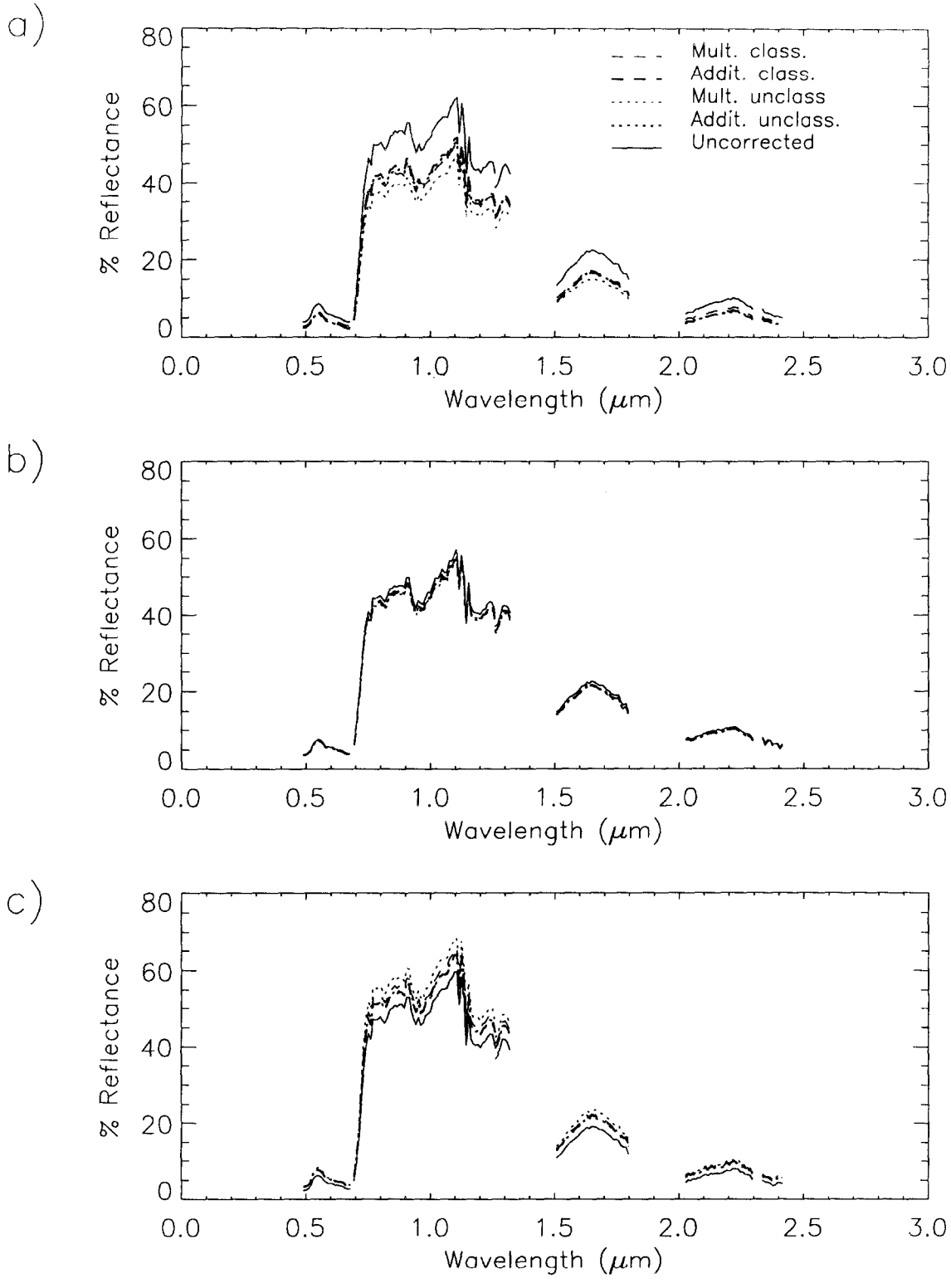

Figure 8. Extracted spectra for test regions in the original image and in images resultant from all four compensation methods. Each spectrum represents the average from nine adjacent pixels. Plotted are spectra from Class 2 a) in the backscatter region of the image, b) near nadir, and c) in the forward scatter region of the image.

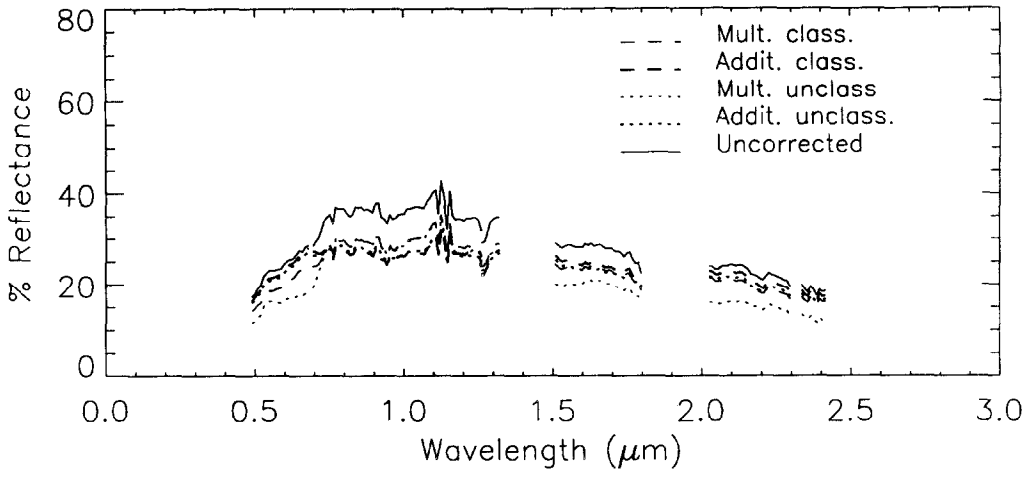

Figure 9. Extracted spectra for a nearly-pure soil test region from Class 1. Note that all compensation methods fail to adequately maintain spectral shape in the 0.6–0.9 μm region.

did display quite marked variations with wavelength in the magnitudes of both $m_{(stddv)}$ and $i_{(stddv)}$ (Fig. 5). If data from those two categories are accepted as indicators of underlying view-angle properties, then it was evident that neither the assumptions of the additive nor multiplicative compensation methods were exclusively valid across wavelengths.

In the chlorophyll absorption region, the strength of a multiplicative relationship [$m_{(stddv)}$] rose (Fig. 5a) as the strength of Effect 1 (q', Fig. 3b) increased, suggesting that Effect 1 may be a multiplicative effect. This suggestion is supported by the theory which states that Effect 1 is driven by the difference in brightness between the upper and lower canopy. Because brightness in a canopy likely follows an exponential extinction rule, the brightness at a given depth in the canopy will always be related in a proportional manner to the brightness at the top of the canopy, and hence the strength of Effect 1 should also be proportional to the brightness at the top of the canopy.

Comparing Results from the Four Methods

The compensation methods tested here represent four strategies to reduce error in reported radiance caused by view-angle-dependent phenomena. As has been shown in this study, the view-angle effect exhibited in a pixel in a given waveband image will depend on that pixel's view-angle, its surface structure, and its brightness. We can express this conceptually in a simple formula:

$$v(a,y)=[b\times f_{type}(a)]+C_{type},$$

where $v(a,y)$ is the brightness effect for a particular pixel, b is some measure of that pixel's inherent brightness, $f_{type}(a)$ is a function describing the response to changes in view-angle for surface type equal to *type* at view-angle a, and C_{type} is the additive component of view-angle effect for *type*. An ideal compensation method would account for all variations across an image b, $f_{type}(a)$, and C_{type}. In practice, however, average values must be used, and thus error in compensation for a pixel will be determined by the separation between the averaged compensation factor and the true view-angle effect for that pixel.

The four methods differ in how they average these values. For the additive methods tested here, b was an average value for the whole scene. Error in compensation for a given pixel will increase as that pixel's brightness increasingly departs from this average brightness. This error is especially evident in the minority soil-dominated class (Class 1) in this vegetation-dominated scene, but also appears in the vegetated classes because Class 2 and 3 differed in average brightness. Multiplicative methods alleviate this problem by using the pixel's starting brightness as an estimate of b. Therefore, the multiplicative-unclassified method performed better than the additive-unclassified method, although Class 1 still suffered in the chlorophyll absorption region.

The latter observation is explained by the averaging of $f_{type}(a)$ and C_{type} in the multiplicative unclassified method. Unclassified methods treated the whole image as a single *type*. Because vegetation dominated the scene, both $f_{type}(a)$ and C_{type} were average values heavily influenced by vegetation. When these were applied to Class 1, which showed unique view-angle responses in all of the interpretive coefficients, the compensation was inaccurate. By classifying into three groups, the gross variations in $f_{type}(a)$ and C_{type} were accounted for and the errors introduced from compensation were lessened.

Because the multiplicative-classified method allowed the most variability in b, $f_{type}(a)$, and C_{type}, theoretically it should have been the most successful method. While this appears to be true, especially in the maintenance of spectral integrity, the distinctions were minimal between it and the additive-classified and multiplicative-unclassi-

fied methods. Only the additive-unclassified method displayed blatantly inappropriate brightness compensation.

Summary of Results

Given the results of this study, several general statements can be made about view-angle brightness effects:

1. Surface BRDF is the primary determinant of view-angle effects in this scene. In theory, atmospheric path radiance should play some role; indeed, the presence of an additive component in the view-angle response hints at the presence of path radiance. However, most of the wavelength-dependent changes in view-angle response are attributed to surface characteristics.
2. Kimes' theory (Kimes, 1983) of BRDF describes the view-angle responses. For closed vegetative canopies, Effect 1 dominates, and there is little variation between closed canopies of high and low structural complexity. For open or sparsely vegetated canopies, Effect 2 dominates.
3. In terms of view-angle compensation, the manifested view-angle effect for a given surface is a function of both the brightness of the surface and the magnitude of Effects 1 and 2 for that surface, all of which vary considerably from surface to surface. A successful compensation method will account for these variations across an image, although gross approximations appear to perform adequately.

CONCLUSIONS

For most of the surfaces involved in this study, the use of empirical view-angle compensation strategies appeared to unmask the information content in this vegetation-dominated scene. Because soil and vegetation have quite different BRDF effects, it is expected that this technique may be less effective in environments with substantial subpixel soil/vegetation mixing.

Although several simplifying assumptions were needed to conduct this study, they do not appear to have prevented adequate view-angle brightness compensation. Inaccuracies in curve-fitting caused by spatial autocorrelation, insufficient degrees of polynomial fitting, or inaccurate atmospheric correction algorithms could not be quantified, but the success of the methods appeared to indicate that their role was subordinate to other factors. When used intelligently, then, these fairly simple empirical methods can be efficient preprocessing tools in situations where view-angle effects mask information content.

This research was funded by the Terrestrial Ecology Program, Office of Mission to Planet Earth, NASA (NAGW-4880), as part of the MODLERS project. Additional support was provided by the NSF-sponsored H. J. Andrews Forest LTER Program (BSR 90-11663). We thank three anonymous reviewers for their time and helpful comments.

REFERENCES

Abuelgasim, A. A., and Strahler, A. H. (1994), Modeling bidirectional radiance measurements collected by the Advanced Solid-State Array Spectroradiometer (ASAS) over Oregon Transect Conifer Forests. *Remote Sens. Environ.* 47:261–275.

Brown, R. J., Bernier, M., and Fedosojevs, G. (1982), Geometrical and atmospheric considerations of NOAA AVHRR imagery. In *1982 Machine Processing of Remotely Sensed Data Symposium*, Purdue University Press, West Lafayette, IN, pp. 374–381.

Cihlar, J., Manak, D., and Voisin, N. (1994), AVHRR bidirectional reflectance effects and compositing. *Remote Sens. Environ.* 48:77–88.

Daughtry, C. S. T., Biehl, L. L., and Ranson, K. J. (1989), A new technique to measure the spectral properties of conifer needles. *Remote Sens. Environ.* 27:81–91.

Deering, D. W., Middleton, E. M., and Eck, T. F. (1994), Reflectance anisotropy for a spruce-hemlock forest canopy. *Remote Sens. Environ.* 47:242–260.

Gao, B.-C., Heidebrecht, K. A., and Goetz, A. F. H. (1993), Derivation of scaled surface reflectance from AVIRIS data. *Remote Sens. Environ.* 44(2):165–178.

Grier, C. C., and Logan, R. S. (1977), Old-growth Douglas fir communities of a western Oregon watershed: biomass distribution and production budgets. *Ecol. Monogr.* 47(4): 373–400.

Hugli, H., and Frei, W. (1981), Correcting for anisotropic reflectances in remotely sensed images from mountainous terrains. In *1981 Machine Processing of Remotely Sensed Data Symposium*, Purdue University Press, West Lafayette, IN, pp. 363–374.

Irons, J. R., and Labovitz, M. L. (1982), A data analytic approach to look-angle radiance adjustment. *J. Appl. Photogr. Eng.* 8(3):128–137.

Irons, J. R., Johnson, B. L., Jr., and Linebaugh, G. H. (1987), Multiple-angle observations of reflectance anisotropy from an airborne linear array sensor. *IEEE Trans. Geosci. Remote Sens.* GE-25(3):372–383.

Irons, J. R., Ranson, K. J., Williams, D. L., Irish, R. R., and Huegel, F. G. (1991), An off-nadir-pointing imaging spectroradiometer for terrestrial ecosystem studies. *IEEE Trans. Geosci. Remote Sens.* 29(1):66–74.

Johnson, L. F. (1994), Multiple view zenith angle observations of reflectance from ponderosa pine stands. *Int. J. Remote Sens.* 15(18):3859–3865.

Kimes, D. S. (1983), Dynamics of directional reflectance factor distributions for vegetation canopies. *Appl. Opt.* 22(9): 1364–1372.

Kimes, D. S., Newcomb, W. W., Nelson, R. F., and Schutt, J. B. (1986), Directional reflectance distributions of a hardwood and pine forest canopy. *IEEE Trans. Geosci. Remote Sens.* GE-24(2):281–293.

Kleman, J. (1987), Directional reflectance factor distributions for two forest canopies. *Remote Sens. Environ.* 23:83–96.

Kriebel, K. T. (1978), Measured spectral bidirectional reflec-

tion properties of four vegetated surfaces. *Appl. Opt.* 17(2):253–259.

Leckie, D. G. (1987), Factors affecting defoliation assessment using airborne multispectral scanner data. *Photogramm. Eng. Remote Sens.* 53(12):1665–1674.

Leckie, D. G., Beaubein, J., Gibson, J. R., O'Neill, N. T., Piekutowski, T., and Joyce, S. P. (1995), Data processing and analysis for MIFUCAM: a trial of MEIS imagery for forest inventory mapping. *Can. J. Remote Sens.* 21(3):337–356.

Li, X., and Strahler, A. H. (1986), Geometric-optical bidirectional reflectance modeling of a conifer forest canopy. *IEEE Trans. Geosci. Remote Sens.* GE-24(6):906–919.

Martin, M. E. (1994), Measurements of foliar chemistry using laboratory and airborne high spectral resolution visible and infrared data, Ph.D. dissertation, University of New Hampshire.

Martin, M. E., Newman, S. D., Aber, J. D., and Congalton, R. (1996), Determining forest species composition using high spectral resolution remote sensing data. In *Summaries of the Sixth Annual JPL Airborne Earth Science Workshop* (R. O. Green, Ed.), Jet Propulsion Laboratory, Pasadena, CA.

Nalepka, R. F., and Morgenstern, J. P. (1972), Signature extension techniques applied to multispectral scanner data. In *Proc. of the Eighth Int. Symp. on Remote Sens. of Environ.*, 2–6 Oct. 1972, Environmental Research Institute of Michigan, Ann Arbor, MI, Vol. II, pp. 881–893.

Norman, J. M., Welles, J. M., and Walter, E. A. (1985), Contrasts among bidirectional reflectance of leaves, canopies, and soils. *IEEE Trans. Geosci. Remote Sens.* GE-23(5): 659–667.

Qi, J., Moran, M. S., Cabot, F., and Dedieu, G. (1995), Normalization of sun/view angle effects using spectral albedo-based vegetation indices. *Remote Sens. Environ.* 52:207–217.

Ranson, K. J., Biehl, L. L., and Bauer, M. E. (1985), Variations in spectral response of soybeans with respect to illumination, view, and canopy geometry. *Int. J. Remote Sens.* 6(12):1827–1842.

Ranson, K. J., Irons, J. R., and Williams, D. L. (1994), Multispectral bidirectional reflectance of northern forest canopies with the advanced solid-state array spectroradiometer (ASAS). *Remote Sens. Environ.* 47:276–289.

Royer, A., Vincent, P., and Bonn, F. (1985), Evaluation and correction of viewing angle effects on satellite measurements of bidirectional reflectance. *Photogramm. Eng. Remote Sens.* 51(12):1899–1914.

Staenz, K., Ahern, F. J., and Brown, R. J. (1981), The influence of illumination and viewing geometry on the reflectance factor of agricultural targets. In *Proc. of the Fifteenth Int. Symp. on Remote Sens. of Environ.*, 11–15 May 1981, Environmental Research Institute of Michigan, Ann Arbor, MI, pp. 867–882.

Staenz, K., Meyer, P., Itten, K. I., Goodenough, D. G., and Teillet, P. M., (1986), Viewing angle corrections of airborne multispectral scanner data acquired over forested surfaces. In *Proc. of IGARSS 1986 Symposium*, European Space Agency Pub. Div., Noordwijk, The Netherlands, pp. 671–676.

Teillet, P. M., Goodenough, D. G., Fedosejevs, G., Byers, R., and Marjama, L. (1985), Radiometric limitations to thematic mapper image information content. In *Proc. of ACSM-ASPRS Fall Convention*, Indianapolis, IN, ACSM and ASPRS, Falls Church, VA, pp. 892–901.

Treitz, P. M., Howarth, P. J., and Leckie, D. G. (1985), The capabilities of two airborne multispectral sensors for classifying coniferous forest species. In *Proc. of the Nineteenth Int. Symp. on Remote Sens. of Environ.*, 21–25 Oct. 1985, Environmental Research Institute of Michigan, Ann Arbor, MI, pp. 335–350.

Vane, G., Green, R. O., Chrien, T. G., Enmark, H. T., Hansen, E. G., and Porter, W. M. (1983), The Airborne Visible/Infrared Imaging Spectrometer (AVIRIS). *Remote Sens. Environ.* 44(2/3):127–144.

Walthall, C. L., Norman, J. M., Welles, J. M., Campbell, G., and Blad, B. L. (1985), Simple equation to approximate the bidirectional reflectance from vegetative canopies and bare soil surfaces. *Appl. Opt.* 24(3):383–387.

Williams, D. L. (1991), A comparison of spectral reflectance properties at the needle, branch, and canopy level for selected conifer species. *Remote Sens. Environ.* 35:79–93.